Biosensors and Bioelectronics 124–125 (2019) 33–39

Contents lists available at ScienceDirect

Biosensors and Bioelectronics

journal homepage: www.elsevier.com/locate/bios

Perovskite-type $BiFeO_3$/ultrathin graphite-like carbon nitride nanosheets p-n heterojunction: Boosted visible-light-driven photoelectrochemical activity for fabricating ampicillin aptasensor

Lan Ge[a], Yuhuan Xu[a], Lijun Ding[a], Fuheng You[a], Qian Liu[a,*], Kun Wang[a,b,**]

[a] Key Laboratory of Modern Agriculture Equipment and Technology, School of Chemistry and Chemical Engineering, Jiangsu University, Zhenjiang 212013, PR China
[b] Key Laboratory of Sensor Analysis of Tumor Marker, Ministry of Education, College of Chemistry and Molecular Engineering, Qingdao University of Science and Technology, Qingdao 266042, PR China

ARTICLE INFO

Keywords:
Ultrathin graphite-like carbon nitride
$BiFeO_3$ nanoparticle
Heterojunction
Photoelectrochemical aptasensor
Ampicillin

ABSTRACT

Developing effective sensing method for trace analysis of ampicillin (AMP) is urgent and significant due to its residue possess serious threats to human health. Herein, a p-n heterojunction, on the basis of p-type $BiFeO_3$ nanoparticles coupled n-typed ultrathin graphite-like carbon nitride (utg-C_3N_4) nanosheets, has been designed and synthesized via a simple electrostatic interaction strategy. Such p-n heterojunction has two advantages: one is capable to narrow the band gap of photoactive materials from 2.20 eV of $BiFeO_3$ down to 2.04 eV of $BiFeO_3$/utg-C_3N_4, leading to improve the efficiency of visible light utilization; and the other is to facilitate the charge separation rate, resulting in the boosted photoelectrochemical (PEC) performance of $BiFeO_3$/utg-C_3N_4. Under visible light illumination, the photocurrent of the resulted $BiFeO_3$/utg-C_3N_4 was 7.0-fold enhanced than that of pure $BiFeO_3$ nanoparticles, and indeed 2.3-fold enhanced comparing to $BiFeO_3$/bulk-C_3N_4. Based on excellent PEC properties of $BiFeO_3$/utg-C_3N_4, an on-off-on PEC aptasensor was successfully fabricated for ampicillin (AMP) determination with highly selectivity and sensitivity. The fabricated PEC aptasensor exhibited excellent PEC performance with a broad linear in the range from 1×10^{-12} mol L^{-1} to 1×10^{-6} mol L^{-1} as well as a low detection limit of 3.3×10^{-13} mol L^{-1} (S/N = 3), and also good feasibility in real sample. The excellent analytical performance indicated that PEC aptasensor on the basis of the visible light driven $BiFeO_3$/utg-C_3N_4 heterojunction can provide a promising biosensor platform for sensitive detection AMP in food and environment analysis.

1. Introduction

Ampicillin (AMP), a β-lactam antibiotic of penicillin family-like drug with highly activity against most gram-positive and anaerobic pathogens, has been widely used in medicine and agriculture to treat bacterial infections (Iranifam and Kharameh, 2014; Fernandez-Gonzalez et al., 2003). However, excessive use of AMP in animal husbandry and agriculture inevitably cause residue in dairy food products, and threat human health such as allergic reactions, breathing difficulties, and seizures in humans (Song et al., 2012). The U.S. Food and Drug Administration had issued maximum residue limits (MRLs) for AMP about 10 μg/L (about 2.8×10^{-8} mol L^{-1}) (Ang et al., 1997). The MRLs for AMP was specified as 50 μg/L (about 1.40×10^{-7} mol L^{-1}) (Gai et al., 2017) in China. The traditional analytical methods of AMP have previously been explored, such as high performance liquid chromatography (Tolhurst et al., 1996), surface-enhanced Raman scattering (Andreou et al., 2015), fluorescence (Song et al., 2012), chemiluminescence (Iranifam et al., 2014) and electrochemical (Wang et al., 2016b). Although, various classical methods due to its accuracy has been widely applied for the analysis of AMP, each of these methods usually has at least one restriction, such as time-consuming operation procedures, expensive equipment and professional technical skills. Thus, fabricating a simple, rapid and low-cost method is necessary for the analysis of AMP with good specificity and high sensitivity.

The photoelectrochemical (PEC) sensor has received considerable attentions in analytical performance and biodetection applications (Shu and Tang, 2017; Zhao et al., 2014). Because of the separation of the light source and the electrochemical signal, the PEC sensor has many

* Corresponding author.
** Corresponding author at: Key Laboratory of Modern Agriculture Equipment and Technology, School of Chemistry and Chemical Engineering, Jiangsu University, Zhenjiang 212013, PR China.
E-mail addresses: liuqian@ujs.edu.cn (Q. Liu), wangkun@ujs.edu.cn (K. Wang).

https://doi.org/10.1016/j.bios.2018.09.093
Received 18 July 2018; Received in revised form 27 September 2018; Accepted 27 September 2018
Available online 28 September 2018
0956-5663/

advantages including desirable sensitivity, low background signal, short analytical time and simple instrumentation setup (Li et al., 2016; Qiu et al., 2018; Shu et al., 2018). Different from traditional electrochemical analysis, photoactive materials based on the high photoelectric conversion efficiency and the unique biological compatibility is required by the design of PEC biosensor (Zhuang et al., 2015). Meanwhile, the essential of PEC biosensors is the use of photoactive materials as sensing species to convert photo irradiation into electrical signals, and the intensity of the light source directly determines the photoelectric conversion efficiency (Okoth et al., 2016). However, the UV light, which only accounts for 2–4% of solar energy, is a high-energy excitation light source that easily resulting in fatal damage toward biomolecules (Ge et al., 2018). Therefore, the development of nontoxic and high efficient visible light responsive photoactive material is necessary and beneficial for fabricating PEC aptasensor. Recently, perovskite-type $BiFeO_3$ has attracted considerable interest owing to its nontoxicity and good chemical stability (Gao et al., 2007; Ruhle et al., 2012). $BiFeO_3$ with a narrow bandgap of 2.2 eV is a p-type semiconductor, which has been considered as one of the third-generation visible light-responsive photoactive materials (Dong et al., 2015; Humayun et al., 2016). However, $BiFeO_3$ possess poorly rated the PEC activity owing to the rapid recombination of photoinduced electrons and holes (Zhou et al., 2018). Several strategies have been devoted to enhance the photoactivity of $BiFeO_3$, such as heterojunction constructing (Kong et al., 2016), elemental doping (Wang et al., 2016a, 2016b) and $BiFeO_3$-based nanocomposites synthetizing (Soltani and Lee, 2016).

The metal-free graphitic-like carbon nitride (g-C_3N_4) as a kind of n-type semiconductor has possessed nontoxic, photoelectrical, appropriate band gap, chemical stability, high thermal stability and other properties (She et al., 2016; Zhang et al., 2017). The coupling of g-C_3N_4 with other semiconductors to constructing heterostructures is an effective method to promote the charge separation efficiency. g-C_3N_4/Bi_2WO_6 (Wang et al., 2017a; Wu et al., 2018; Da Silva et al., 2017; Lv et al., 2017). However, the PEC property of bulk g-C_3N_4 is poor owing to rapid recombination rate of photoinduced carriers and low quantum efficiency (Wu et al., 2018). Nevertheless, compared to bulk g-C_3N_4, the ultrathin g-C_3N_4 (utg-C_3N_4) displayed a superior PEC performance by virtue of its ultrahigh charge separation efficiency and larger surface area (Zhang et al., 2013). Zhu et al. synthetized Pt/utg-C_3N_4 suggesting that the utg-C_3N_4 can be utilized as photoactive support and provide more ideas into developing visible light responsive electrode (Zhu et al., 2017b). Chen et al. prepared utg-C_3N_4/WO_3 heterojunction nanocomposite offering an effective strategy to improve charge separation efficiency and enhancing PEC performance (Chen et al., 2016).

Herein, a p-n heterojunction $BiFeO_3$/utg-C_3N_4 based on p-type $BiFeO_3$ nanoparticles coupling with n-type utg-C_3N_4 nanosheets was synthesized by a facile electrostatic strategy. Due to the introduction of utg-C_3N_4, the construction of p-n heterojunction can be capable to boost the charge separation efficiency, resulting in enhanced visible-light-driven PEC activity compared with $BiFeO_3$ and $BiFeO_3$/bulk-C_3N_4. On the basis of this, an on-off-on PEC aptasensor was developed for high sensitivity detection of AMP. This investigation extended the application scope of $BiFeO_3$/utg-C_3N_4 p-n heterostructure, which could be a promising approach to fabricate PEC aptasensor for the analysis of AMP in real sample.

2. Experimental section

2.1. Reagents and chemicals

Melamine ($C_3H_6N_6$), bismuth nitrate [$Bi(NO_3)_3{\cdot}5H_2O$], iron nitrate [$Fe(NO_3)_3{\cdot}9H_2O$], ethylene glycol, methanol, 2-methoxyethanol and citric acid (CA) were obtained from Sinopharm Chemical Reagent Co., Ltd. The DNA aptamer for AMP was synthesized by Shanghai Sangon Biotech Co., Ltd. with the following sequence: 5′-TTT TGC GGG CGG TTG TAT AGC GG-3′. Ampicillin (AMP), tetracycline (TC), chloramphenicol (CAP), sulfadimethoxine (SDM), amoxicillin (AMO) were acquired from Aladin Reagent Co., Ltd. (Shanghai, China). 0.1 mol L^{-1} phosphate buffered saline (PBS, pH 7.4) was employed as the supporting electrolyte 0.01 mol L^{-1} Tris − HCl buffer (pH 7.4) was used for the preparation of DNA aptamer stock solutions. Double distilled water was used throughout experiment. Other reagents of analytical grade and used as received without further purification.

2.2. Preparation of $BiFeO_3$/utg-C_3N_4

Preparation of $BiFeO_3$: $BiFeO_3$ nanoparticles were prepared by a typical sol-gel way according to the previously reported literatures with minor modification (Zhu et al., 2014). In a routine procedure, 0.002 mol of $Bi(NO_3)_3{\cdot}5H_2O$ and 0.002 mol of $Fe(NO_3)_3{\cdot}9H_2O$ were dissolved in a beaker containing of 20 mL of 2-methoxyethanol, then 20 μL of 0.1 mol L^{-1} HNO_3 was added into the solution. Subsequently, the mixture solution was added into 0.002 mol of CA as a complexing agent and 10 mL of ethylene glycol as dispersion agent and stirred for 1 h at 60 °C to from a sol, which was then dried at 150 °C to form the gel powder. Finally, the powder was calcined at 500 °C for 2 h at a temperature rate of 2 °C min^{-1} to obtained $BiFeO_3$ nanoparticles.

Preparation of utg-C_3N_4 was according to the previously reported literatures (Chen et al., 2016). (Detailed information was provided in Supplementary materials.)

Preparation of $BiFeO_3$/utg-C_3N_4: different amounts of utg-C_3N_4 with $BiFeO_3$ were scattered in methanol with ultrasonic agitation for 2 h. The forming the mixture solution was agitated in the draught cupboard for 20 h. Finally, the as-prepared $BiFeO_3$/utg-C_3N_4 was dried at 80 °C for the following use. To study the effect of utg-C_3N_4 amount on PEC performance, various mass rations of utg-C_3N_4 from 10% to 50% were prepared using the similar procedure. For comparison, $BiFeO_3$/bulk-C_3N_4 was prepared by the similar method.

2.3. Fabrication of the modified electrodes

Firstly, the ITO electrodes were cleaned with 1 mol L^{-1} of NaOH solution and followed by washing with ultrasonication in deionized water and alcohol until clean, respectively. Then, 5 mg of $BiFeO_3$/utg-C_3N_4 were dispersed ultrasonically in 1 mL H_2O to get 5 mg mL^{-1} $BiFeO_3$/utg-C_3N_4 suspension. 40 μL of the $BiFeO_3$/utg-C_3N_4 suspension were coated on ITO electrode surface with a fixed area of 0.5 cm^2 and then dried in air at room temperature to obtain $BiFeO_3$/utg-C_3N_4 modified ITO electrode (denoted as $BiFeO_3$/utg-C_3N_4/ITO). For comparison, utg-C_3N_4/ITO, $BiFeO_3$/ITO and $BiFeO_3$/bulk-C_3N_4/ITO were obtained using the similar steps, respectively.

2.4. Fabrication of the PEC aptasensor

The process of fabricating AMP PEC aptasensor was as follows, 20 μL of AMP aptamer solution (4×10^{-6} mol L^{-1}) was decorated on the $BiFeO_3$/utg-C_3N_4/ITO electrode. The prepared aptamer/$BiFeO_3$/utg-C_3N_4/ITO were aired at room temperature and thoroughly washed with 0.1 mol L^{-1} PBS to eliminate excess no adsorbed aptamers. 20 μL of AMP solutions with various concentrations were dropped onto the aptamer/$BiFeO_3$/utg-C_3N_4/ITO electrode in ambient air and then followed by rinsing thoroughly with PBS (0.1 mol L^{-1}). Finally, the apatsensor was successfully fabricated and applied for AMP detection.

2.5. Photoelectrochemical measurement

All PEC experiments were performed on a CHI760E electrochemical workstation (Shanghai Chenhua Instrument Co. Ltd., China) with Xe lamp (250 W, CHF-XM35–500W, Beijing Chang tuo) as the visible light irradiation source (passing through a 400 nm UV-cut filter). A standard three-electrode system was carried out with the whole PEC experiments

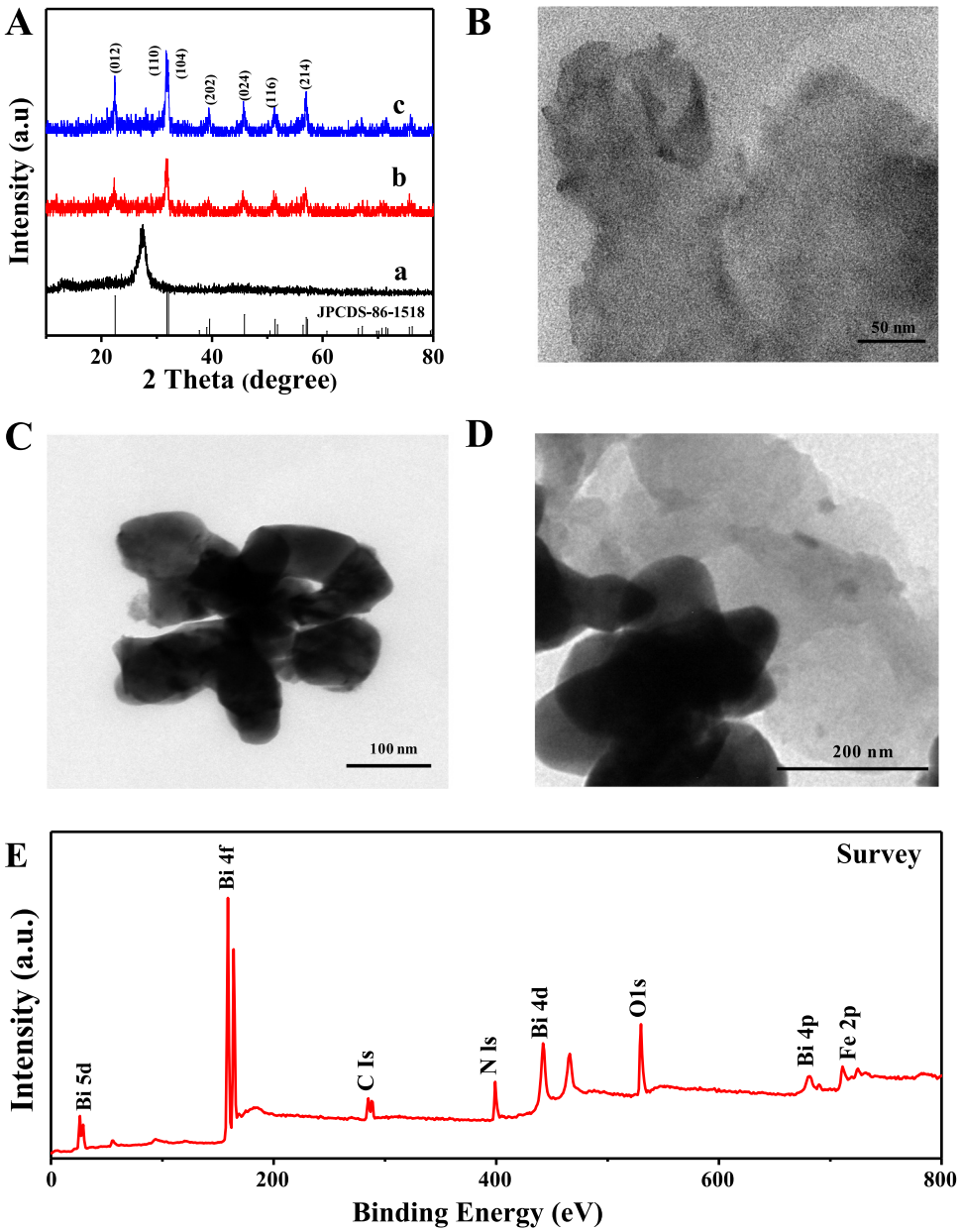

Fig. 1. (A) XRD patterns of utg-C_3N_4 (a), $BiFeO_3$ (b), $BiFeO_3$/utg-C_3N_4 (c); TEM images of (B) utg-C_3N_4, (C) $BiFeO_3$ and (D) $BiFeO_3$/utg-C_3N_4 and (E) XPS survey of $BiFeO_3$/utg-C_3N_4.

in 0.1 mol L^{-1} PBS at 0 V, where the fabricated ITO as the working electrode, a platinum (Pt) wire as the auxiliary electrode, and a saturated calomel electrode (SCE) as the reference electrode. Electrochemical impedance spectroscopy (EIS) were carried out on the KCl (0.1 mol L^{-1}) solution containing $[Fe(CN)_6]^{3-/4-}$ (5 mmol L^{-1})with the frequency range from 10^{-1} Hz to 10^5 Hz.

3. Results and discussion

3.1. Characterization of the samples

The crystalline property of the utg-C_3N_4, $BiFeO_3$ and $BiFeO_3$/utg-C_3N_4 were investigated by XRD patterns in Fig. 1A. For the utg-C_3N_4, the diffraction peaks (2θ) at 13.0° and 27.2° could be clearly observed (curve a), which correspond to the (100) and (002), respectively (Bai et al., 2014). The XRD pattern of $BiFeO_3$ (curve b) displays reflection peaks corresponding to the rhombohedral perovskite structure with the *R*3c space group (JCPDS No. 86-1518) and no impurity peaks were detected, indicating high crystalline quality of the obtained samples (Wang et al., 2016a, 2016b). Notably, the XRD pattern of $BiFeO_3$/utg-C_3N_4, the characteristic peaks indexing to utg-C_3N_4 was not detected due to relatively small amount and uniform dispersion of utg-C_3N_4 (Wu et al., 2018).

The morphologies of the utg-C_3N_4, $BiFeO_3$, $BiFeO_3$/bulk-C_3N_4 and $BiFeO_3$/utg-C_3N_4 were characterized by TEM. Fig. 1B displays the TEM image of utg-C_3N_4, and ultrathin sheet-like structures was observed. The TEM image of pure $BiFeO_3$ shown Fig. 1C indicated the $BiFeO_3$ nanoparticles has irregular shape morphology with a particle size of 100–200 nm. Fig. S1 shows that $BiFeO_3$ nanoparticles coupled the surface of bulk-C_3N_4 which has a bulk structure with stacking layer. Moreover, the TEM image of $BiFeO_3$/utg-C_3N_4 can be clearly seen that the $BiFeO_3$ nanoparticles were attached to the surface of utg-C_3N_4 nanosheets (Fig. 1D), indicating a heterojunction was formed.

XPS were performed to prove the chemical property and element constituent of the as-synthesized $BiFeO_3$/utg-C_3N_4. As can be seen, Fig. 1E exhibited the survey XPS that $BiFeO_3$/utg-C_3N_4 were consisted

of Bi, Fe, O, C and N elements, respectively. Three peaks at 158.8 eV and 164.1 eV can be associated with Bi $4f_{7/2}$ and Bi $4f_{5/2}$ (Zhu et al., 2017a) (Fig. S2A). The Fe 2p peaks observed at 711.0 eV and 724.5 eV were assigned to Fe $2p_{3/2}$ and Fe $2p_{1/2}$ (Liu et al., 2017) (Fig. S2B). The spectrum of O 1s was displayed in Fig. S2C, three peaks were located at 529.6 eV, 531.1 eV and 532.2 eV, which corresponding to Bi/Fe-O, C=O and C-O-C, respectively (Chen et al., 2018). The high resolution C 1s peak (Fig. S2D) can be deconvoluted into two main peaks at binding energies of 284.9 eV and 288.5 eV, representing C-C and N-C-N coordination (Chen et al., 2016). The N 1s XPS spectrum displayed three main peaks at binding energies of 398.9 eV, 399.3 eV and 400.7 eV, respectively (Fig. S2E), which were attributed to the C-N=C, N-C_3 and C-N-H (Chen et al., 2018). The results above demonstrated that the $BiFeO_3$/utg-C_3N_4 was successfully synthesized.

Fig. S3 displays the zeta potentials of utg-C_3N_4, $BiFeO_3$, and $BiFeO_3$/utg-C_3N_4 heterojunction. As shown, the zeta potentials of utg-C_3N_4 and $BiFeO_3$ were − 27.0 mV (curve a) and + 20.8 mV (curve b); after the heterojunction formation, the zeta potential of $BiFeO_3$/utg-C_3N_4 was − 16.9 mV (curve c), indicating the $BiFeO_3$/utg-C_3N_4 heterojunction was formed via the electrostatic reaction. Based on the investigation above, the possible formation mechanism of $BiFeO_3$/utg-C_3N_4 was presented as follows: the utg-C_3N_4 nanosheets would serve as a substrate to induce the adsorption of the $BiFeO_3$ nanoparticles through electrostatic reaction, and the relevant formation procedure was portrayed in Scheme 1A.

3.2. Photoelectrochemical measurements

Fig. 2A displays the photocurrent intensity of different modified electrodes under visible light irradiation. The weak photocurrent response of 0.064 μA (curve a) and 0.033 μA (curve b) was exhibited for pure utg-C_3N_4 and $BiFeO_3$ modified electrode. Then the photocurrent intensity of the $BiFeO_3$/utg-C_3N_4/ITO electrode was 0.23 μA, which was about 3.6-fold enhanced than that of utg-C_3N_4/ITO electrode and 7.0-fold than that of $BiFeO_3$/ITO. It could be explained that the p-n heterojunction could accelerate the charge transfer and effectively curb the rapid recombination of charge carrier, leading to enhancing photocurrent response. Furthermore, the photocurrent intensity of the $BiFeO_3$/utg-C_3N_4/ITO was 2.3-fold enhancement compared with $BiFeO_3$/bulk-C_3N_4 indicating utg-C_3N_4 could effectively accelerate charge transfer comparing to bulk-C_3N_4 (Chen et al., 2016). To further understand the interface charge transfer process of the as-prepared samples, EIS analysis of the pure utg-C_3N_4, $BiFeO_3$, $BiFeO_3$/bulk-C_3N_4 and $BiFeO_3$/utg-C_3N_4 were discussed. As can be seen in Fig. 2B, the electron-transfer resistance (R_{et}) value of utg-C_3N_4/ITO, $BiFeO_3$/ITO and $BiFeO_3$/utg-C_3N_4/ITO was about 83, 96 and 69 Ω, respectively, indicating that the formation of p-n heterojunction can accelerate electron transfer rate and restrain charge carrier recombination. The R_{et} of $BiFeO_3$/utg-C_3N_4 was smaller than $BiFeO_3$/bulk-C_3N_4 implying that utg-C_3N_4 possess good electrical conductivity which can facilitate electron transfer comparing to bulk-C_3N_4 (Zhang, 2015).

The UV–visible absorption spectra of pure utg-C_3N_4, $BiFeO_3$,

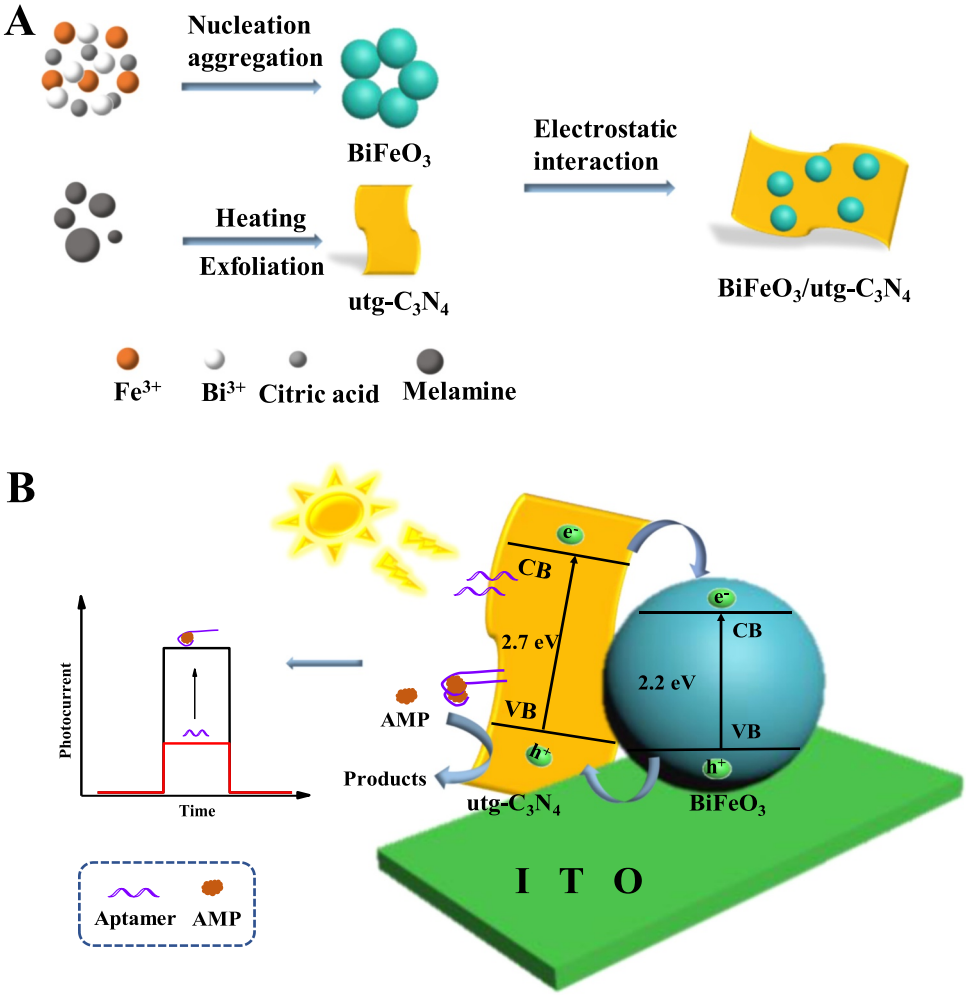

Scheme 1. (A) Schematic diagram for the formation of $BiFeO_3$/utg-C_3N_4 heterojunction and (B) The schematic drawing illustrating of the as-fabricated PEC AMP aptasensor based on $BiFeO_3$/utg-C_3N_4 heterojunction.

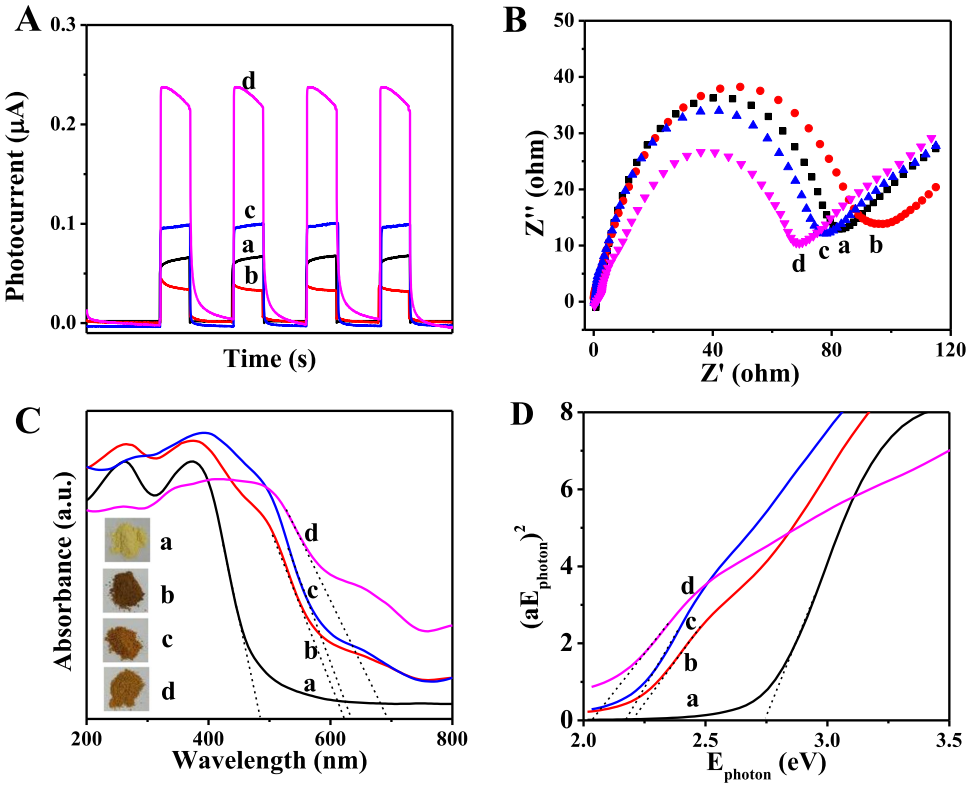

Fig. 2. (A) Photocurrent signals of different electrodes in 0.1 mol L^{-1} PBS at bias potential of 0 V, (B) Nyquist plots of different electrodes in 0.1 mol L^{-1} KCl solution containing 5 mmol L^{-1} $[Fe(CN)_6]^{3-/4-}$, (C) UV–vis diffuse reflectance spectra and (D) Plots of $(Ah\upsilon)^2$ versus the energy ($h\upsilon$) for the band gap energy of different materials: utg-C_3N_4/ITO (a), $BiFeO_3$/ITO (b), $BiFeO_3$/bulk-C_3N_4/ITO (c), and $BiFeO_3$/utg-C_3N_4/ITO (d).

$BiFeO_3$/bulk-C_3N_4 and $BiFeO_3$/utg-C_3N_4 are depicted Fig. 2C. As shown, the absorption band edge of pristine utg-C_3N_4 and $BiFeO_3$ was about 480 nm and 610 nm which was basically consistent with the relative values published in previous reports, respectively (She et al., 2016; Papadas et al., 2015). Moreover, the $BiFeO_3$/utg-C_3N_4 displays broader absorption comparing with $BiFeO_3$ and $BiFeO_3$/bulk-C_3N_4 implying enhance absorption properties in the visible range. Based on the $(\alpha h\upsilon)^2$ versus ($h\upsilon$) plots in Fig. 2D, the bandgaps of utg-C_3N_4, $BiFeO_3$ and $BiFeO_3$/bulk-C_3N_4were estimated to be 2.7 eV, 2.2 eV and 2.17 eV, respectively (Gao et al., 2007; She et al., 2016). Meanwhile, the bandgap of $BiFeO_3$/utg-C_3N_4 was reduced to 2.04 eV, which was narrower than pure utg-C_3N_4, $BiFeO_3$ and $BiFeO_3$/bulk-C_3N_4. The enhanced absorption and narrowed bandgap was beneficial to enhance the visible light activity of $BiFeO_3$/utg-C_3N_4 heterojunction.

3.3. Fabrication of the "on-off-on" PEC aptasensor

The schematic representation of the possible mechanism of PEC aptasensor for specific detection of AMP were shown in Scheme 1B. Under visible-light illumination, both utg-C_3N_4 and $BiFeO_3$ are easily motivated, the photogenerated electrons and hole can be separated and the p-n heterojunction reforming band edge can accelerate electron transfer rate, leading to enhanced PEC performance. The photogenerated electrons on the conduction band (CB) of utg-C_3N_4 are moved to the CB of $BiFeO_3$, then the holes on the valence band (VB) of $BiFeO_3$ may transfer to the VB of utg-C_3N_4. When AMP molecules are present, the aptamer immobilized on $BiFeO_3$/utg-C_3N_4/ITO can specifically interact with AMP on the platform of PEC aptasensor. The photogenerated holes can directly oxidize AMP molecules that from complex with the aptamers, the recombination rate of photoinduced electrons and holes are suppressed and the photoinduced electrons are driven to the counter electrode. Therefore, the presence of AMP molecules can promote the generation of higher photocurrent compared to the absence of AMP.

Fig. 3A presents the photocurrent signal of different modified electrodes. The $BiFeO_3$/utg-C_3N_4 nanocomposites (curve a) displayed a photocurrent of 0.23 μA to get "switch on" state. When the aptamer was

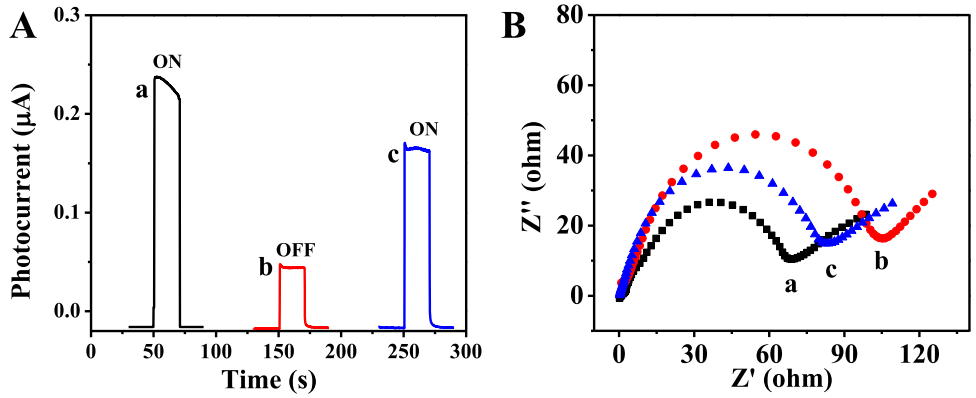

Fig. 3. (A) The PEC curves of different electrodes in 0.1 mol L^{-1} PBS at bias potential of 0 V and (B) Nyquist plots of different electrodes in 0.1 mol L^{-1} KCl solution containing 5 mmol L^{-1} $[Fe(CN)_6]^{3-/4-}$: $BiFeO_3$/utg-C_3N_4/ITO (a), aptamer/$BiFeO_3$/utg-C_3N_4/ITO (b) and AMP/aptamer/$BiFeO_3$/utg-C_3N_4/ITO (c).

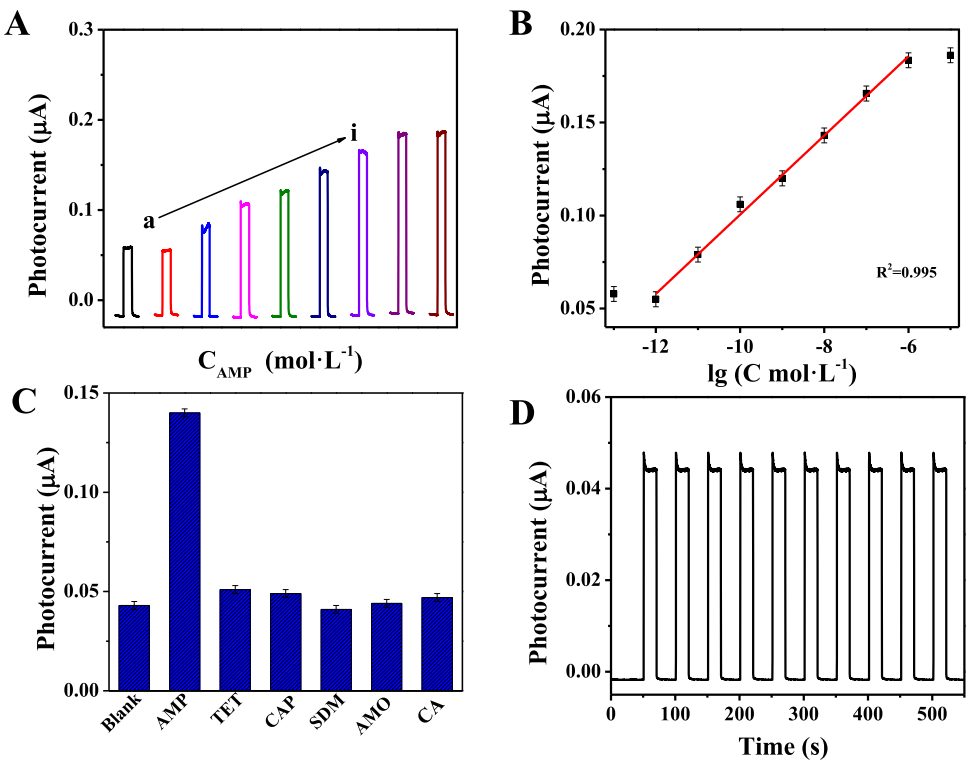

Fig. 4. (A) Photocurrent responses of the fabricating aptasensor at different concentrations of AMP in 0.1 mol L^{-1} PBS at bias potential of 0 V: (a) 10^{-13}, (b) 10^{-12}, (c) 10^{-11}, (d) 10^{-10}, (e) 10^{-9}, (f) 10^{-8}, (g) 10^{-7}, (h) 10^{-6}, (i) 10^{-5} mol L^{-1}, (B) Corresponding calibration curve for AMP detection, (C) Photocurrent responses of the fabricating aptasensor toward other antibiotics at 1×10^{-8} mol L^{-1} and (D) Measurement of stability of the fabricating aptasensor under ten on/off illumination cycles.

introduced, the photocurrent intensity (curve b) remarkably decreased due to the presence of aptamers which enhanced the steric hindrance of the electrode interface and block the electrons transfer (Yan et al., 2015). As a result, the "switch off" state was got, a low PEC background signal was obtained for the further detection of AMP. In the presence of AMP molecules, the photocurrent intensity significantly enhanced (curve c) and the "switch on" state was obtained. It can be explained the reason that the photoinduced holes can directly oxidize AMP molecules and the recombination of photoinduced electrons-holes pairs were restrained.

To further investigate the interfacial charge transfer condition of the stepwise assembly procedure of PEC aptasensor, EIS analysis was employed. Fig. 3B exhibits the R_{et} of each electrode related to the aptasensor. The equivalent circuit applied for fitting the EIS date (Fig. S6), where R_{et}, Z_w, R_s, and Q represent electron transfer resistance, Warburg impedance, electrolyte solution resistance, and constant phase elements, respectively. The AMP aptamers were anchored on $BiFeO_3$/utg-C_3N_4/ITO electrode, the increase of value R_{et} from 68.2 to 105.8 Ω, which was attributed to that aptamers were successfully coated onto the $BiFeO_3$/utg-C_3N_4 electrode. In the presence of AMP molecules, the aptasensor could specifically capture the AMP molecules, the R_{et} of AMP/aptamer-$BiFeO_3$/utg-C_3N_4/ITO (curve c) decreased to 83.3 Ω, confirming the formation of a complex between aptamer and AMP (Okoth et al., 2017). The discussion above indicated the proposed "on-off-on" PEC aptasensor was successfully constructed and could be utilized to the specific and sensitive analysis of AMP.

3.4. Optimization of experimental conditions

To construct the highly efficient and sensitive PEC aptasensor, some experimental parameters influencing PEC response can be supposed to optimize. Different content of utg-C_3N_4 in the heterojunction may influence the PEC activity of the heterojunction, which should be optimized at first. The PEC signals of the $BiFeO_3$/utg-C_3N_4 with different utg-C_3N_4 contents were presented in Fig. S4A. It could be seen clearly that the PEC response of the $BiFeO_3$/utg-C_3N_4 with 30% utg-C_3N_4 was better than others. Therefore, 30% $BiFeO_3$/utg-C_3N_4 was picked as the ideal photo response material for the fabrication of the aptasensor.

Also, the concentration of the aptamer has a remarkably influence on PEC activity of the fabricated aptasensor. Fig. S4B displays that the PEC signal decreased with the increase of the aptamer concentration from 1×10^{-7} to 4×10^{-6} mol L^{-1} and reached a plateau when up to 4×10^{-6} mol L^{-1}. Therefore, 4×10^{-6} mol L^{-1} was adopted as the optimized concentration of aptamer and applied for the aptasensor construction.

3.5. Selective and sensitive PEC aptasensor of AMP

On the basis of the excellent PEC activity of $BiFeO_3$/utg-C_3N_4, the constructed PEC aptasensor was employed to the sensitive detection of AMP. Fig. 4A displays the PEC photocurrent of aptamer-$BiFeO_3$/utg-C_3N_4 modified electrodes to AMP with variable concentrations, and the PEC signal obviously increased with the increase of the concentrations of AMP. The aptasensor exhibited the good linear to the logarithm of AMP concentration in range of 1×10^{-12} mol L^{-1} to 1×10^{-6} mol L^{-1} (Fig. 4B). The regression equation is determined as $I = 0.12174 + 0.02128$ lg[C_{AMP} (mol L^{-1})], with a correlation coefficient $R^2 = 0.995$. In addition, the limit of detection was calculated to be 3.3×10^{-13} mol L^{-1} (defined as $S/N = 3$). The broader liner response and lower detection limit was achieved compared to those previous literatures for AMP determination (Table S1).

The specificity of the fabricated PEC aptasensor should be verified, 1×10^{-8} mol L^{-1} of four other antibiotics as interference, namely, TET, CAP, SDM, AMO and food additives (CA)on the PEC response were explored. As shown in Fig. 4C, different from AMP the other antibiotics did not show significant PEC response on the aptamer- $BiFeO_3$/utg-C_3N_4/ITO electrode, which indicated that the fabricated PEC aptasensor exhibited high specificity for AMP determination.

As depicted in Fig. 4D, the PEC response of the proposed aptasensor was recorded under ten times switching irradiation cycles, and no apparent change occur exhibiting that the as-fabricated PEC aptasensor were fair stability. Furthermore, the PEC aptasensor were stored under 4 °C for 3 weeks, the photocurrent signal of the aptasensor retained 95.4%, indicating the proposed aptasensor possess the good long-term stability (Fig. S5). In addition, the relative standard deviation (RSD) of

Table 1
Measurement results of AMP in milk samples by the PEC method ($n = 3$).

Sample	Spiked (mol L^{-1})	Found (mean[a] ± SD[b])	Recovery (%)	RSD (%)
1	0	0	–	–
2	1.0×10^{-9}	$9.96 (\pm 0.03) \times 10^{-10}$	99.6	3.2
3	1.0×10^{-8}	$1.02 (\pm 0.42) \times 10^{-8}$	102.0	2.7
4	1.0×10^{-7}	$9.97 (\pm 0.38) \times 10^{-8}$	99.7	4.1

[a] Mean, average value of three tests.
[b] SD, standard deviation.

4.9% was achieved compared with a batch of newly prepared aptamer-$BiFeO_3$/utg-C_3N_4/ITO electrodes, proving that the fabricated aptasensor possess excellent reproducibility for the analysis of AMP.

3.6. Real sample analysis

The applicability of the fabricated PEC aptasensor was further explored to the real sample analysis. The milk samples were selected as the real sample, which adding different concentrations of AMP. We pretreat the milk samples according to the literature (Ang et al., 1997). Briefly, 2 mL milk, 0.5 mL of trichloroacetic acid solution (20%) and 0.5 mL of acetonitrile was mixed placed into Teflon centrifuge tube. Then the mixture was mixed and centrifugation, the known amounts of AMP were added into the supernatant. Next, the supernatant reacted with trichloroacetic acid solution and formaldehyde solution at 100 °C for 30 min, cooled to room temperature, and made up to 2 mL with acetonitrile. The supernatant was collected and passed through a filter with a pore size of 45 μm. The recovery test was investigated adopting standard addition method. Table 1 presented these results that the recoveries were observed in the range of 99.6–102.0% with the RSD of 2.7–4.1% suggesting the feasibility of proposed PEC aptasensor for AMP detection in real samples.

4. Conclusions

In summary, a PEC aptasensor was fabricated by employing the p-n type $BiFeO_3$/utg-C_3N_4 heterojunction as visible light responsive photoactive material. The charge separation efficiency and visible light absorption efficiency of photoactive material were promoted significantly by the formation of p-n type heterojunction. Due to the combination of high-performance PEC aptasensor with specificity aptamer, the fabricating PEC aptasensor exhibited a broader liner range (1×10^{-12} mol L^{-1} to 1×10^{-6} mol L^{-1}) and a lower detection limit (3.3×10^{-13} mol L^{-1}). Furthermore, satisfactory results were obtained when the fabricated PEC aptasensor was used for AMP detection in real milk samples. This work not only displays the potentially attractive of the $BiFeO_3$/utg-C_3N_4 photoactive heterojunction in PEC related application, but also provides a novel PEC sensing platform for food, biomedical and environment analysis.

Acknowledgements

This research was supported under the National Natural Science Foundation of China (Nos. 21375050, 21675066 and 61601204), Provincial Natural Science Foundation of Jiangsu (No. BK20160542), the Research Foundation of Zhenjiang Science and Technology Bureau (No. NY2016011) and the Foundation of Key Laboratory of Sensor Analysis of Tumor Marker, Ministry of Education, Qingdao University of Science and Technology (No. SATM201807).

Appendix A. Supporting information

Supplementary data associated with this article can be found in the online version at doi:10.1016/j.bios.2018.09.093

References

Andreou, C., Mirsafavi, R., Moskovits, M., Meinhart, C.D., 2015. Analyst 140, 5003–5005.
Ang, C.Y.W., Luo, W.H., Call, V.L., H, F.R., 1997. J. Agric. Food Chem. 45, 4351–4536.
Bai, X.J., Zong, R.L., Li, C.X., Liu, D., Liu, Y.F., Zhu, Y., 2014. Appl. Catal. B: Environ. 147, 82–91.
Chen, D.Y., Jiang, D., Du, X.J., Zhou, L., Huang, L.Y., Qian, J., Liu, Q., Hao, N., Li, Y.P., Wang, K., 2016. Electrochim. Acta 215, 305–312.
Chen, W., Jiang, D., Zhu, M.Y., Shi, T.Y., Li, H.N., Wang, K., 2018. J. Alloy. Compd. 741, 1203–1211.
Da Silva, G.T.S.T., Carvalho, K.T.G., Lopes, O.F., Ribeiro, C., 2017. Appl. Catal. B: Environ. 216, 70–79.
Dong, G.Z., Fan, H.Q., Tian, H.L., Fang, J.W., Li, Q., 2015. RSC Adv. 5, 29618–29623.
Fernandez-Gonzalez, A., Badia, R., Diaz-Garcia, M.E., 2003. Anal. Chim. Acta 484, 223–231.
Gai, P.P., Gu, C.C., Hou, T., Li, F., 2017. Anal. Chem. 89, 2163–2169.
Gao, F., Chen, X.Y., Yin, K.B., Dong, S., Ren, Z.F., Yuan, F., Yu, T., Zou, Z.G., Liu, J.M., 2007. Adv. Mater. 19, 2889–2892.
Ge, L., Li, H.N., Du, X.J., Zhu, M.Y., Chen, W., Shi, T.Y., Hao, N., Liu, Q., Wang, K., 2018. Biosens. Bioelectron. 111, 131–137.
Humayun, M., Zada, A., Li, Z.J., Xie, M.Z., Zhang, X.L., Qu, Y., Raziq, F., Jing, L.Q., 2016. Appl. Catal. B: Environ. 180, 219–226.
Iranifam, M., Kharameh, M.K., 2014. Luminescence 29, 679–683.
Kong, J.J., Rui, Z.B., Wang, X.Y., Ji, H.B., Tong, Y.X., 2016. Chem. Eng. J. 302, 552–559.
Li, L., Zhang, Y., Zhang, L., Ge, S.G., Liu, H.Y., Ren, N., Yan, M., Yu, J.H., 2016. Anal. Chem. 88, 5369–5377.
Liu, P.D., Sun, H.J., Liu, X.F., Sui, H.T., Zhang, Y., Zhou, D.G., Guo, Q.H., Ruan, Y., 2017. J. Am. Ceram. Soc. 100, 3540–3549.
Lv, S.Z., Li, Y., Zhang, K.Y., Lin, Z.Z., Tang, D.P., 2017. ACS Appl. Mater. Interfaces 9, 38336–38343.
Okoth, O.K., Yan, K., Liu, Y., Zhang, J.D., 2016. Biosens. Bioelectron. 86, 636–642.
Okoth, O.K., Yan, K., Zhang, J.D., 2017. Carbon 120, 194–202.
Papadas, I., Christodoulides, J.A., Kioseoglou, G., Armatas, G.S., 2015. J. Mater. Chem. A 3, 1587–1593.
Qiu, Z.L., Shu, J., Tang, D.P., 2018. Anal. Chem. 90, 1021–1028.
Ruhle, S., Anderson, A.Y., Barad, H.N., Kupfer, B., Bouhadana, Y., Rosh-Hodesh, E., Zaban, A., 2012. J. Phys. Chem. Lett. 3, 3755–3764.
She, X.J., Liu, L., Ji, H.Y., Mo, Z., Li, Y.P., Huang, L.Y., Du, D.L., Xu, H., Li, H.M., 2016. Appl. Catal. B: Environ. 187, 144–153.
Shu, J., Tang, D.P., 2017. Chem. Asian J. 12, 2780–2789.
Shu, J., Qiu, Z.L., Lv, S.Z., Zhang, K.Y., Tang, D.P., 2018. Anal. Chem. 90, 2425–2429.
Soltani, T., Lee, B.-K., 2016. Chem. Eng. J. 306, 204–213.
Song, K.M., Jeong, E., Jeon, W., Cho, M., Ban, C., 2012. Anal. Bioanal. Chem. 402, 2153–2161.
Tolhurst, T.A., N, A., Libelt, B., Woods, E.F., Levine, B.S., 1996. Chromatographia 42, 223–226.
Wang, J.J., Tang, L., Zeng, G.M., Deng, Y.C., Liu, Y.N., Wang, L.L., Zhou, Y.Y., Guo, Z., Wang, J.J., Zhang, C., 2017a. Appl. Catal. B: Environ. 209, 285–294.
Wang, S., Chen, D., Niu, F., Zhang, N., Qin, L.S., Huang, Y.X., 2016a. J. Alloy. Compd. 688, 399–406.
Wang, X.Z., Dong, S.S., Gai, P.P., Duan, R., Li, F., 2016b. Biosens. Bioelectron. 82, 49–54.
Wu, Y., Wang, H., Tu, W.G., Liu, Y., Tan, Y.Z., Yuan, X.Z., Chew, J.W., 2018. J. Hazard. Mater. 347, 412–422.
Yan, K., Liu, Y., Yang, Y.H., Zhang, J.D., 2015. Anal. Chem. 87, 12215–12220.
Zhang, H., 2015. ACS Nano 9, 9451–9469.
Zhang, K.Z., Lv, S.Z., Lin, Z.Z., Tang, D.P., 2017. Biosens. Bioelectron. 95, 34–40.
Zhang, X.D., Xie, X., Wang, H., Zhang, J.J., Pan, B.C., Xie, Y., 2013. J. Am. Chem. Soc. 135, 18–21.
Zhao, W.W., Xu, J.J., Chen, H.Y., 2014. Chem. Rev. 114, 7421–7441.
Zhou, Q., Lin, Y.X., Zhang, K.Y., Li, M.J., Tang, D.P., 2018. Biosens. Bioelectron. 101, 146–152.
Zhu, A.S., Zhao, Q.D., Li, X.Y., Shi, Y., 2014. ACS Appl. Mater. Interfaces 6, 671–679.
Zhu, M.S., Zhai, C.Y., Sun, M.J., Hu, Y.F., Yan, B., Du, Y.K., 2017b. Appl. Catal. B: Environ. 203, 108–115.
Zhu, M.Y., Liu, Q., Chen, W., Yin, Y.Y., Ge, L., Li, H.N., Wang, K., 2017a. ACS Appl. Mater. Interfaces 9, 38832–38841.
Zhuang, J.Y., Lai, W.Q., Xu, M.D., Zhou, Q., Tang, D.P., 2015. ACS Appl. Mater. Interfaces 7, 8330–83388.